Journal of Visualized Experiments

Lumped-parameter and finite element modeling of heart failure with preserved ejection fraction

--Manuscript Draft--

Article Type:	Invited Methods Collection - JoVE Produced Video
Manuscript Number:	JoVE62167R2
Full Title:	Lumped-parameter and finite element modeling of heart failure with preserved ejection fraction
Corresponding Author:	Ellen Roche Massachusetts Institute of Technology Cambridge, MA UNITED STATES
Corresponding Author's Institution:	Massachusetts Institute of Technology
Corresponding Author E-Mail:	etr@mit.edu
Order of Authors:	Luca Rosalia
	Caglar Ozturk
	Ellen Roche
Additional Information:	
Question	**Response**
Please specify the section of the submitted manuscript.	Engineering
Please indicate whether this article will be Standard Access or Open Access.	Standard Access (US$2,400)
Please indicate the **city, state/province, and country** where this article will be **filmed**. Please do not use abbreviations.	Cambridge, MA, USA
Please confirm that you have read and agree to the terms and conditions of the author license agreement that applies below:	I agree to the Author License Agreement
Please provide any comments to the journal here.	

TITLE:

Lumped-parameter and Finite Element Modeling of Heart Failure with Preserved Ejection Fraction

AUTHORS AND AFFILIATIONS:

Luca Rosalia[1,2], Caglar Ozturk[1], Ellen T. Roche[1,2,3]

[1]Institute for Medical Engineering and Science, Massachusetts Institute of Technology, Cambridge, Massachusetts 02139, USA
[2]Health Science and Technology Program, Harvard/Massachusetts Institute of Technology, Cambridge, Massachusetts 02139, USA
[3]Department of Mechanical Engineering, Massachusetts Institute of Technology, Cambridge, Massachusetts 02139, USA

L.R. and C.O. contributed equally to this work.

Luca Rosalia (lros@mit.edu)
Caglar Ozturk (cozturk@mit.edu)

Corresponding author:
Ellen T. Roche (etr@mit.edu)

KEYWORDS:

Lumped-parameter model, Windkessel model, finite element model, living heart model, cardiovascular system, aortic stenosis, heart failure, heart failure with preserved ejection fraction, HFpEF

SUMMARY:

This work introduces two computational models of heart failure with preserved ejection fraction based on a lumped-parameter approach and finite element analysis. These models are used to evaluate the changes in the hemodynamics of the left ventricle and related vasculature induced by pressure overload and diminished ventricular compliance.

ABSTRACT:

Scientific efforts in the field of computational modeling of cardiovascular diseases have largely focused on heart failure with reduced ejection fraction (HFrEF), broadly overlooking heart failure with preserved ejection fraction (HFpEF), which has more recently become a dominant form of heart failure worldwide. Motivated by the paucity of HFpEF computational models, two distinct computational models are presented in this paper to simulate the hemodynamics of HFpEF resulting from left ventricular pressure overload. First, an object-oriented lumped-parameter model was developed using a numerical solver. This model is based on a zero-dimensional (0D) Windkessel-like network, which depends on the geometrical and mechanical properties of the constitutive elements and offers the advantage of low computational costs. Second, a finite element analysis (FEA) software package was utilized for the implementation of a

multidimensional simulation. The FEA model combines three-dimensional (3D) multiphysics models of the electro-mechanical cardiac response, structural deformations, and fluid cavity-based hemodynamics and utilizes a simplified lumped-parameter model to define the flow exchange profiles among different fluid cavities. Through each approach, both the acute and chronic hemodynamic changes in the left ventricle and proximal vasculature resulting from pressure overload were successfully simulated. Specifically, pressure overload was modeled by reducing the orifice area of the aortic valve, while chronic remodeling was simulated by reducing the compliance of the left ventricular wall. Consistent with the scientific and clinical literature of HFpEF, results from both models show (i) an acute elevation of transaortic pressure gradient between the left ventricle and the aorta and a reduction in the stroke volume and (ii) a chronic decrease in the end-diastolic left ventricular volume, indicative of diastolic dysfunction. Finally, the FEA model demonstrates that stress in the HFpEF myocardium is remarkably higher than in the healthy heart tissue throughout the cardiac cycle.

INTRODUCTION:

Heart failure is a leading cause of death worldwide, which occurs when the heart is unable to pump or fill adequately to keep up with the metabolic demands of the body. The ejection fraction, i.e., the relative amount of blood stored in the left ventricle that is ejected with each contraction is used clinically to classify heart failure into (i) heart failure with reduced ejection fraction (HFrEF) and (ii) heart failure with preserved ejection fraction (HFpEF), for ejection fractions less than or greater than 45%, respectively[1-3]. Symptoms of HFpEF often develop in response to left ventricular pressure overload, which can be caused by several conditions including aortic stenosis, hypertension, and left ventricular outflow tract obstruction[3-7]. Pressure overload drives a cascade of molecular and cellular aberrations, leading to thickening of the left ventricular wall (concentric remodeling) and ultimately, to wall stiffening or loss of compliance[8-10]. These biomechanical changes profoundly affect cardiovascular hemodynamics as they result in an elevated end-diastolic pressure–volume relationship and in a reduction of the end-diastolic volume[11].

Computational modeling of the cardiovascular system has advanced the understanding of blood pressures and flows in both physiology and disease and has fostered the development of diagnostic and therapeutic strategies[12]. In silico models are classified into low- or high-dimensional models, with the former utilizing analytical methods to evaluate global hemodynamic properties with low computational demand and the latter providing a more extensive multiscale and multiphysics description of cardiovascular mechanics and hemodynamics in the 2D or 3D domain[13]. The lumped-parameter Windkessel representation is the most common among the low-dimensional descriptions. Based on the electrical circuit analogy (Ohm's law), this mimics the overall hemodynamic behavior of the cardiovascular system through a combination of resistive, capacitive, and inductive elements[14]. A recent study by this group has proposed an alternative Windkessel model in the hydraulic domain that allows the modeling of changes in the geometry and mechanics of large vessels—heart chambers and valves—in a more intuitive way than traditional electrical analog models. This simulation is developed on an object-oriented numerical solver (see the **Table of Materials**) and can capture the normal hemodynamics, physiologic effects of cardiorespiratory coupling, respiratory-driven

blood flow in single-heart physiology, and hemodynamic changes due to aortic constriction. This description expands upon the capabilities of lumped-parameter models by offering a physically intuitive approach to model a spectrum of pathologic conditions including heart failure[15].

High-dimensional models are based on FEA to compute spatiotemporal hemodynamics and fluid-structure interactions. These representations can provide detailed and accurate descriptions of the local blood flow field; however, due to their low computational efficiency, they are not suitable for studies of the entire cardiovascular tree[16,17]. A software package (see the **Table of Materials**) was employed as an anatomically accurate FEA platform of the 4-chamber adult human heart, which integrates the electro-mechanical response, structural deformations, and fluid cavity-based hemodynamics. The adapted human heart model also comprises a simple lumped-parameter model that defines the flow exchange among the different fluid cavities, as well as a complete mechanical characterization of the cardiac tissue[18,19].

Several lumped-parameter and FEA models of heart failure have been formulated to capture hemodynamic abnormalities and evaluate therapeutic strategies, particularly in the context of mechanical circulatory assist devices for HFrEF[20-24]. A broad array of 0D lumped-parameter models of various complexities has therefore successfully captured the hemodynamics of the human heart in physiological and HFrEF conditions via optimization of two or three-element electrical analog Windkessel systems[20,21,23,24]. The majority of these representations are uni- or biventricular models based on the time varying-elastance formulation to reproduce the contractile action of the heart and use a non-linear end-diastolic pressure–volume relationship to describe ventricular filling[25-27]. Comprehensive models, which capture the complex cardiovascular network and mimic both the atrial and ventricular pumping action, have been used as platforms for device testing. Nevertheless, although a significant body of literature exists around the field of HFrEF, very few in silico models of HFpEF have been proposed[20,22,28-31].

A low-dimensional model of HFpEF hemodynamics, recently developed by Burkhoff et al.[32] and Granegger et al.[28], can capture the pressure-volume (PV) loops of the 4-chamber heart, fully recapitulating the hemodynamics of various phenotypes of HFpEF. Furthermore, they utilize their in silico platform to evaluate the feasibility of a mechanical circulatory device for HFpEF, pioneering computational research of HFpEF for physiology studies as well as device development. However, these models remain unable to capture the dynamic changes in blood flows and pressures observed during disease progression. A recent study by Kadry et al.[30] captures the various phenotypes of diastolic dysfunction by adjusting the active relaxation of the myocardium and the passive stiffness of the left ventricle on a low-dimensional model. Their work provides a comprehensive hemodynamic analysis of diastolic dysfunction based on both the active and passive properties of the myocardium. Similarly, the literature of high-dimensional models has primarily focused on HFrEF[19,33-37]. Bakir et al.[33] proposed a fully-coupled cardiac fluid-electromechanics FEA model to predict the HFrEF hemodynamic profile and the efficacy of a left-ventricular assist device (LVAD). This biventricular (or two-chamber) model utilized a coupled Windkessel circuit to simulate the hemodynamics of the healthy heart, HFrEF and HFrEF with LVAD support[33,37].

Similarly, Sack et al.[35] developed a biventricular model to investigate right ventricular dysfunction. Their biventricular geometry was obtained from a patient's magnetic resonance imaging (MRI) data, and the model's finite-element mesh was constructed using image segmentation to analyze the hemodynamics of a VAD-supported failing right ventricle[35]. Four-chamber FEA cardiac approaches have been developed to enhance the accuracy of models of the electromechanical behavior of the heart[19,34]. In contrast to biventricular descriptions, MRI-derived four-chamber models of the human heart provide a better representation of the cardiovascular anatomy[18]. The heart model employed in this work is an established example of a four-chamber FEA model. Unlike lumped-parameter and biventricular FEA models, this representation captures hemodynamic changes as they occur during disease progression[34,37]. Genet et al.[34], for example, used the same platform to implement a numerical growth model of the remodeling observed in HFrEF and HFpEF. However, these models evaluate the effects of cardiac hypertrophy on structural mechanics only and do not provide a comprehensive description of the associated hemodynamics.

To address the lack of HFpEF in silico models in this work, the lumped-parameter model previously developed by this group and the FEA model were readapted to simulate the hemodynamic profile of HFpEF. To this end, the ability of each model to simulate cardiovascular hemodynamics at baseline will be first demonstrated. The effects of stenosis-induced left ventricular pressure overload and of diminished left ventricular compliance due to cardiac remodeling—a typical hallmark of HFpEF—will then be evaluated.

PROTOCOL:

1. 0D lumped-parameter model

1.1. Simulation setup

NOTE: In the numerical solver environment (see the **Table of Materials**), construct the domain as shown in **Figure 1**. This is composed of the 4-chamber heart, the upper body, abdominal, lower body, and thoracic compartments, as well as the proximal vasculature, including the aorta, the pulmonary artery, and the superior and inferior venae cavae. The standard elements used in this simulation are part of the default hydraulic library. Details can be found in the **Supplemental Files**.

1.1.1. Navigate the hydraulics library to find the required elements: hydraulic pipeline, constant volume hydraulic chamber, linear resistance, centrifugal pump, check valve, variable area orifice, and the custom hydraulic fluid.

1.1.1.1. Drop the hydraulic pipeline elements into the workspace.

NOTE: These account for frictional losses as well as wall compliance and fluid compressibility in blood vessels and heart chambers. Through this block, the pressure loss is calculated using the Darcy-Weisbach law, whereas the change in diameter due to wall compliance depends on the compliance proportionality constant, the luminal pressure, and the time constant. Finally, fluid

compressibility is defined by the bulk modulus of the medium.

1.1.1.2. Insert the constant volume hydraulic chamber elements to define wall compliance and fluid compressibility.

NOTE: This block does not take into account pressure losses due to friction.

1.1.1.3. Add the linear resistance elements to define resistance to flow.

NOTE: This is independent of the geometrical properties of the vasculature, analogously to the resistive element used in electrical analog Windkessel models. Other blocks, such as the centrifugal pump, the check valve, the variable-area orifice, and the custom hydraulic fluid elements should be inserted to generate the desired pressure input to the system, model the effects of heart valves on blood flow, and define the mechanical properties of blood. Through these elements, the behavior of the cardiovascular system in both physiology and disease can be fully captured. The input signal for the centrifugal pump can be found in **Figure S1A**.

1.1.1.4. Model the contractility of each heart chamber through the custom variable-compliance compliance chamber element.

NOTE: This accepts compliance as a time-varying user-defined input signal and is based on the time-varying elastance model (**Figure S1B–D**).

1.1.2. Provide the parameters relative to each element, as shown in **Table S1**, also found in Rosalia et al.[15]

1.1.3. Insert a Physical Signal (PS) Repeating Sequence element for each of the blocks that require a time-varying user-defined input signal: the LV pump, the variable-compliance compliance elements, and the variable-area orifice blocks.

NOTE: Input signals utilized for this simulation can be found in **Figure S1.**

1.1.4. Select the default **ODE 23t implicit solver** and run the simulation for 100 s to reach a steady state.

2. The FEA model

2.1. Simulation setup

NOTE: The FEA Model utilizes a coupled electrical-mechanical analysis in sequence. In this model, the electrical analysis is conducted first; then the resulting electric potentials are used as the excitation source in the following mechanical analysis. Therefore, the simulation setup contains two work domains: the electrical (**ELEC**) and the mechanical (**MECH**) domains, that are predefined in the FEA simulation software (**Table of Materials**)[18]. Hence, the following section only describes

the analysis workflow. The FEA model uses the following user subroutines **HETVAL**, **VUANISOHYPER**, and **UAMP** for the electrical and mechanical material modeling[18].

2.1.1. Navigate the **ELEC** domain to perform electrical analysis using the predefined temperature procedure in the **Standard** module.

2.1.1.1. Use a single-analysis step named **BEAT**. Set the duration of the cardiac cycle to 500 ms and apply an electrical potential pulse to a node set representing the sinoatrial (SA) node (**node set: R_Atrium-1.SA_NODE**).

2.1.1.2. Review the default electrical waveform, which ranges from –80 mV to 20 mV over 200 ms with the smooth step amplitude definition, as described in the model guide[18]. Use the default values of material constants in the electrical analysis to adjust the AV delay.

2.1.1.3. Launch the **Job** module, and create a job named **heart-elec**.

2.1.2. Once the electrical analysis setup is completed, navigate the **MECH** domain to perform the fluid cavity-based mechanical analysis.

NOTE: The mechanical simulation is performed after the electrical analysis, and the resulting electric potentials are used as the excitation source for the mechanical analysis. The mechanical analysis contains multiple steps.

2.1.2.1. Use the three main steps named **PRE-LOAD**, **BEAT1**, AND **RECOVERY1**. In the **PRE-LOAD** step, review the boundary conditions of the pre-stressed state of the heart. Use 0.3 s as the step time to linearly ramp up the pressure in the fluid chambers.

NOTE: The predefined fluid cavity pressure values are shown in **Table S3**. The pre-stressed state of the heart was already defined in the normal heart simulation setup, and the initial node conditions are provided in the external simulation files, as listed in **Table S5**. Recalculation of the zero-stress state using the inverse mechanical simulation is required whenever the boundary condition is modified, as explained in steps 3.2.2–3.2.4.

2.1.2.2. In the **BEAT1** step, use 0.5 s as the step time to simulate contraction.

2.1.2.3. In the **RECOVERY1** step, select 0.5 s for cardiac relaxation and ventricular filling for a heart rate of 60 bpm.

2.1.2.4. Enable the subsequent steps, **BEATX** and **RECOVERYX**, to simulate more than one cardiac cycle to reach a steady state.

NOTE: Three cardiac cycles will be sufficient to reach steady state. One cycle of the simulation is completed in ~8 h on a 24-core processor (3.2 GHz x 24).

2.1.2.5. Launch the **Job** module, and create a job named **heart-mech**, enabling the **double precision** option.

2.2. Review simplified lumped-parameter Windkessel model

NOTE: The mechanical domain of the FEA model has a blood flow model, which is based on a simplified lumped-parameter circuit and is created as a combination of surface-based fluid cavities and fluid exchanges as seen in **Figure 2**[18].

2.2.1. Use the Windkessel representation mentioned in the above note to run the simulation. Review the blood flow model representation to adjust the values of the resistive and capacitive elements for flow resistances and structural compliances, respectively.

2.2.2. Review the 3D finite element representation of four heart chambers, and ensure their geometrical positions are accurate.

2.2.3. Check the heart assembly, and switch to the **Interaction** module to adjust the compliance and contractility values of each of the four heart chambers.

NOTE: The default values in the **Interaction** module are configured to simulate an idealized healthy human heart beat cycle[18].

2.2.4. Review the following hydrostatic fluid cavities in the **Interaction** module, CAV-AORTA, CAV-LA, CAV-LV, CAV-PULMONARY_TRUNK, CAV-RA, CAV-RV, CAV-SVC, CAV-ARTERIAL-COMP, CAV-PULMONARY-COMP, and CAV-VENOUS-COMP (**Table S3**).

2.2.5. Use the compliance chambers (CAV-ARTERIAL-COMP, CAV-PULMONARY-COMP, and CAV-VENOUS-COMP) as cubic volumes as they represent the compliance of the arterial, venous, and pulmonary circulations.

2.2.6. Attach three compliance cubic volumes to a grounded spring, and review the stiffness value to model the pressure-volume response in the arterial, venous, and pulmonary circulations.

2.2.7. Check the following fluid exchange definitions between the hydrostatic fluid cavities: arterial-venous, venous-right atrium, right atrium-right ventricle, right ventricle-pulmonary system, pulmonary system-left atrium, left atrium-left ventricle, and left ventricle-aorta (**Table S4**).

2.2.8. Adjust the viscous resistance coefficient to modify the blood flow model in each fluid exchange link (see **Supplemental files** for more information about the viscous resistance effect).

2.3. Multiphysics simulation

2.3.1. Locate the **CAE database** file in the working directory.

NOTE: The FEA Model in this protocol is delivered in the database and is named as **LH-Human-Model-Beta-V2_1.cae**.

2.3.2. Insert the input, object, and library files to the working directory to run the simulation. See **Table S5** for the full list of input and library files.

2.3.3. Launch the FEA model simulation software (see the **Table of Materials**).

NOTE: Consult the software provider for compatibility with later versions[18].

2.3.4. Review the parts, assembly, and boundary conditions in both **ELEC** and **MECH** domains, as described in sections 2.2 and 2.3.

2.3.5. First, run the electrical simulation job named **heart-elec**, as described in section 2.1.1.3. Visually inspect the electrical potential results to verify that the **heart-elec** simulation ran as expected. Then, ensure that the result file **heart-elec.odb** is in the working directory.

2.3.6. Move to the second simulation phase by switching to the **MECH** domain. Review the values of the material constants used in the mechanical simulation to model the desired passive and active cardiac response.

2.3.7. Ensure that the material library files for the mechanical analysis use the **HYBRID-** string name. To modify the material response of the heart chambers, adjust the appropriate hybrid material file, or replace the entire material response by defining a new material behavior in the **Materials** section in the **CAE** module.

NOTE: Detailed information about the built-in constitutive laws can be found in the user guide[18].

2.3.8. In the **PRE-LOAD** step, set the pressures of the hydrostatic cavities to obtain the desired physiologic behavior. Use the built-in smooth amplitude option to ramp up from zero to the desired pressure level as described in step 2.1.2.1.

2.3.9. Disable the pressure boundary conditions defined in 2.1.2.1 to run the blood flow model with a constant overall blood volume within the circulation system. Run the simulation job named **heart-mech**, as described in section 2.1.2.5.

3. Aortic valve stenosis

NOTE: Aortic stenosis is often a driver of HFpEF as it leads to pressure overload and ultimately, to concentric remodeling and compliance loss of the left ventricular wall. The hemodynamics observed in aortic stenosis often progress to those seen in HFpEF.

3.1. The lumped-parameter model

3.1.1. Modify the input signal in the PS repeating sequence element relative to the aortic valve, located in the left ventricular compartment. Simulate a reduction of the orifice area equal to 70% compared to baseline (**Table S6**).

NOTE: The input values will represent the orifice area of the stenotic valve during each heartbeat. The orifice area value can be easily adjusted by multiplying the **start output values** vector of the aortic valve PS element by a decimal value corresponding to the final orifice area with respect to its original value. In this work, a factor of 0.3 was used to achieve 70% constriction.

3.2. The FEA model

3.2.1. Modify the fluid exchange definition of the **LINK-LV-ARTERIAL** parameter.

NOTE: This parameter possesses a viscous resistance coefficient tuned to the blood flow between the left ventricle and the aorta. The effective exchange area can be modified to adjust the blood flow and create the appropriate aortic stenosis model (**Table S7**).

3.2.2. Locate the toolbox folder and copy the files inside that folder to the main working directory.

3.2.3. Perform an inverse mechanical simulation by executing the toolbox files[18]. To this end, change the suction pressures of the left ventricle and left atrium to 6 mmHg in the fluid cavity to adjust their initial volumetric state for the aortic stenosis model. Execute the **inversePreliminary.py** function.

NOTE: Recalculation of the zero-stress state using the inverse mechanical simulation is required whenever the boundary condition is modified.

3.2.4. Once the inverse mechanical simulation is completed, run the post-processing functions: **calcNodeCoords.py** and **straight_mv_chordae.py**. Use the default values for the other flow parameters, and run a new mechanical simulation as described in section 2.1.2.5.

4. HFpEF hemodynamics

NOTE: To simulate the effects of chronic remodeling, the mechanical properties of the left heart were modified.

4.1. The lumped-parameter model

4.1.1. Modify the left ventricular diastolic compliance of the LV compliance element to mimic wall stiffening due to pressure-overload, using the value of end-diastolic compliance in **Table S8**.

NOTE: Assume compliance to drop linearly from end-systole to end-diastole.

4.1.2. Increase the leak resistance of the LV pump to 18×10^6 Pa s m^{-3} (**Table S8**) to capture the elevated left ventricular pressures observed in HFpEF.

4.2. The FEA model

4.2.1. Edit the active material properties of the left ventricle geometry. Increase the stiffness component to tune the active tissue response affecting the stress components in the fiber and sheet directions in the constitutive model.

4.2.1.1. Modify the material response of the left ventricle in the **mech-mat-LV_ACTIVE** file.

NOTE: The magnitude of stiffness for the left ventricular chamber can be tuned to provide the appropriate diastolic compliance effects.

4.2.1.2. Increase the stiffness parameters *a* and *b* in the anisotropic hyperelastic formulation to capture the increased stiffness response for the HFpEF physiology.

4.2.1.3. In the **PRE-LOAD** step, set the fluid cavity pressures of the left ventricle and left atrium to 20 mmHg.

4.2.1.4. Perform an inverse mechanical simulation to obtain the volumetric state of the left ventricle and atrium. Export the nodal coordinates from the **heart-mech-inverse.odb** file[18].

4.2.1.5. Execute the post-processing functions: **calcNodeCoords.py** and **straight_mv_chordae.py**, as described in step 3.2.4. Locate the new nodal input files in the working directory and perform a new mechanical simulation, as described in section 2.1.2.5.

REPRESENTATIVE RESULTS:

Results from the baseline simulations are illustrated in **Figure 3**. This depicts the pressure and volume waveforms of the left ventricle and the aorta (**Figure 3A**) as well as the left ventricular PV loop (**Figure 3B**). The two in silico models show similar aortic and left ventricular hemodynamics, which are within the physiologic range. Minor differences in the response predicted by the two platforms can be noticed during the ventricular emptying and filling phases, where non-linearities are better captured by the FEA model compared to the lumped-parameter platform. In physiology, such non-linear effects arise mainly as a result of the hyperelastic response of the heart tissue and are therefore more accurately reproduced by multidomain and high-order computational models[18].

Ventricular and aortic hemodynamics were obtained for aortic stenosis, as this often leads to left ventricular pressure overload and ultimately, to the development of HFpEF. Pressure and volume waveforms at a 70% reduction of the aortic valve orifice area are shown for both models in **Figure 4**. Stenosis resulted in an elevated pressure gradient across the aortic valve. For the 70% stenosis considered in this work, peak transaortic pressure gradients of 41 mmHg and 54 mmHg were

obtained with the lumped-parameter (**Figure 4A**) and FEA (**Figure 4B**) models, respectively. This moderate variation likely arises as another consequence of the lack of a constitutive equation defining the material properties of the cardiac tissue in the lumped-parameter model, in which compliance is simply defined by an array of numerical values. This model therefore does not capture fluid-structure interactions, which are instead accurately represented by the FEA model. Nevertheless, the results from both models are consistent with the American Society of Echocardiography (ASE) and the European Association of Echocardiography (EAE) classifications of moderate aortic valve stenosis, which denote peak transaortic gradients of 40–65 mmHg for aortic constrictions of approximately 60–75%[38-40].

Left ventricular PV loops at baseline, 70% aortic stenosis, and of HFpEF following stiffening of the ventricular wall are summarized in **Figure 5**. Similar patterns can be observed in **Figure 5A**, depicting the results from the lumped-parameter model, and in **Figure 5B**, which shows the hemodynamics obtained via FEA. These PV loops are consistent with those in the scientific and clinical literature of HFpEF[1,11,28,32]. In particular, both models are able to capture the increase in the systolic left ventricular pressure due to the rise in afterload induced by aortic stenosis. Furthermore, the end-systolic volume is increased in the stenosis PV loop, leading to a drop in stroke volume. Upon remodeling and loss of left ventricular compliance, the end-diastolic pressure-volume relationship (EDPVR) becomes elevated, resulting in higher end-diastolic pressures and lower end-diastolic volumes. These phenomena, which are due to the inability of the left ventricle to relax and fill adequately, are successfully captured by the HFpEF PV loops in both the low- and high-dimensional models.

As another indication for diminished diastolic function, the flow through the mitral valve is shown in **Figure S2**, which highlights both the early relaxation (E) and atrial contraction (A) phases. Compared to the normal and stenosis profiles, HFpEF flow is characterized by a slightly higher peak E-phase mitral flow and significantly diminished peak A-phase flow, highlighting that passive stiffening of the left ventricle results in an elevated E/A ratio, which is consistent with the scientific literature[30]. Finally, **Figure 6** shows changes in the myocardium stress map in the normal and HFpEF hearts during both systole and diastole. The long-axis view of the left ventricle illustrates the volumetric averaged stress distributions and shows elevated stresses in the HFpEF heart due to the characteristic loss of ventricular compliance. From baseline values of (61.1 ± 49.8) kPa and (0.51 ± 7.35) kPa for the healthy heart during peak-systole (t = 0.2 s) and end-diastole (t = 1.0 s), respectively, the mean stress correspondingly increased to (97.2 ± 205.7) kPa and (2.69 ± 16.34) kPa in HFpEF, suggesting that the hemodynamic changes observed in HFpEF are rooted in profound structural changes affecting the failing heart.

FIGURE AND TABLE LEGENDS:

Figure 1: Domain of anatomically derived lumped-parameter model in the object-oriented numerical solver (see the **Table of Materials**), showing the four-chamber heart, the aorta, and the upper body, abdominal, lower body, and pulmonary circulations. Abbreviations: LV = left ventricle; RV = right ventricle; LA = left atrium; RA = right atrium; R1 = arterial resistance; R2 = venous resistance; C = compliance; IVC: inferior vena cava; SVC: superior vena cava.

Figure 2: Finite element analysis model of the human heart. (**A**) 3D representation of the finite element analysis model of the human heart. (**B**) Simplified lumped-parameter representation of the blood flow model in the model coupled with the structural fluid exchange models[18]. Abbreviations: LV = left ventricle; RV = right ventricle; LA = left atrium; RA = right atrium; R_{aortic} = aortic valve resistance; R_{mitral} = mitral valve resistance; $R_{pulmonary}$ = pulmonary valve resistance; $R_{tricuspid}$ = tricuspid valve resistance; $C_{arterial}$ = systemic arterial compliance; R_{system} = systemic arterial resistance; C_{venous} = systemic venous compliance, R_{venous} = systemic venous resistance; $C_{pulmonary}$ = pulmonary compliance; $R_{pulmonary\text{-}system}$ = pulmonary resistance.

Figure 3: Baseline simulations and pressure–volume waveforms for the lumped-parameter and finite element analysis models of the human heart. (**A**) Left ventricular pressure and volume waveforms and aortic pressure calculated by the lumped-parameter and FEA models at baseline. (**B**) Left ventricular PV loop obtained through both platforms at baseline. Abbreviations: FEA = finite element analysis; LV = left ventricular; PV = pressure–volume.

Figure 4: Left ventricular pressure and volume waveforms and aortic pressure calculated at 70% reduction of the aortic valve orifice area. (**A**) Lumped-parameter model, (**B**) FEA model. Abbreviations: FEA = finite element analysis; LV = left ventricular.

Figure 5: Left ventricular PV loops of the healthy heart, under acute stenosis-induced pressure overload, and of the HFpEF heart following chronic remodeling and stiffening. (**A**) Lumped-parameter, (**B**) FEA models. Abbreviations: $EDPVR_H$ = end-diastolic pressure-volume relationship in the simulated healthy heart; $EDPVR_{HFpEF}$: end-diastolic pressure-volume relationship in the simulated HFpEF physiology; PV – pressure–volume; FEA = finite element analysis.

Figure 6: von Mises stress (avg: 75%) under physiologic conditions and of the HFpEF heart during peak-systole and diastole, as predicted by the FEA model. The color maps indicate stress levels in MPa. Higher stresses can be seen in HFpEF (92.7–2.7 kPa) compared to the healthy heart (61.1–0.5 kPa) during peak-systole (t = 0.2 s) and end-diastole (t = 1.0 s).

Figure S1: Input signals for (**A**) centrifugal pump, (**B**) left ventricle, (**C**) right ventricle, (**D**) left and right atria for the lumped-parameter simulation.

Figure S2: (**A**) Aortic and (**B**) mitral flow signals for the baseline, stenosis, and HFpEF profiles, obtained by FEA. Abbreviations: E = early relaxation phase; A = atrial contraction; FEA = finite element analysis; HFpEF = heart failure with preserved ejection fraction.

Table S1. Geometric and mechanical parameters of baseline lumped-parameter simulation.

Table S2. Extensive set of parameters of baseline lumped-parameter simulation.

Table S3. Fluid cavities values in the mechanical finite element analysis (FEA) model[18].

Table S4. Boundary conditions of fluid exchange links for the finite element analysis (FEA) model[18].

Table S5. The required simulation files for the finite element analysis (FEA) model[18].

Table S6. Parameters for the aortic-stenosis lumped-parameter simulation.

Table S7. Fluid exchange link definitions in the finite element analysis (FEA) model[18].

Table S8. Parameters for the HFpEF lumped-parameter simulation.

DISCUSSION:

The lumped-parameter and FEA platforms proposed in this work recapitulated the cardiovascular hemodynamics under physiologic conditions, both in the acute phase of stenosis-induced pressure overload and in chronic HFpEF. By capturing the role that pressure overload plays in the acute and chronic phases of HFpEF development, the results from these models are in agreement with the clinical literature of HFpEF, including the onset of a transaortic pressure gradient due to aortic stenosis, an increase in the left ventricular pressure, and the reduction in the end-diastolic volume due to wall stiffening[41]. Furthermore, this FEA model was able to capture elevations in myocardial stress in HFpEF throughout the cardiac cycle. To ensure a correct setup of these simulations, the steps outlined in the protocol section above must be followed rigorously. For the lumped-parameter model, it is essential that the network of hydraulic elements is recreated correctly as shown in **Figure 1** and that the prescribed values are provided as input parameters (**Table S1** and **Table S2**). In addition, the solver block must be defined and connected to the network at any node.

Functioning of the FEA model requires all the simulation files that are packaged with the solver[18] that are listed in **Table S5**. Omission of any of the prerequisite components might cause early termination of the simulation. For both platforms, it is critical to obtain the baseline simulation with the default input parameters prior to recreating the stenosis and HFpEF hemodynamic profiles. The original research article outlining the baseline simulation[15]and the documentation linked to the simulation in the Supplemental Files can be consulted for troubleshooting the lumped-parameter model. Similarly, this FEA framework contains the software documentation and toolbox folder for troubleshooting[18]. In the event of a simulation error, the user can invoke the simulation diagnostics by executing the relative plug-ins in the toolbox folder[18]. Hemodynamic results from the lumped-parameter model were analogous to those calculated via FEA in each of the simulated conditions and consistent with the clinical literature of HFpEF. The high-dimensional FEA platform allows the capture of the complex biomechanical behavior of the heart and provides an accurate description of cardiovascular hemodynamics, albeit at the expense of the elevated computational demand. However, in the lumped-parameter model, the runtime is reduced from several hours to few minutes, constituting a significant advantage over higher-order in silico models.

In addition, by modeling a larger number of cardiovascular compartments, this lumped-

parameter simulation allows the examination of blood flows and pressures at various sites of the cardiovascular tree and is therefore suitable for studies that extend beyond the heart chambers and the proximal vasculature. However, while being able to recapitulate global hemodynamics, this description fails to capture some minor effects of structural interactions and therefore lacks the accuracy typical of FEA representations. Analysis of the cardiac mechanics obtained in this study through the finite element approach corroborated those from previous investigations. Specifically, these mean stress values are in the same range as those predicted by growth models of the partially supported heart during chronic failure[34,37]. Compared to those models, the stress values found in these studies described herein were moderately higher due to the elevated level of aortic stenosis simulated to induce pressure overload. In addition, it was found that loss of left ventricular compliance in HFpEF has a major impact on endocardial stress.

However, diastolic stiffness and its sensitivity were not parametrically investigated in this study. In fact, this parameter was tuned to capture the physiologically relevant hemodynamic profile of chronic left ventricular pressure overload. Extensive sensitivity analysis should be performed to fully characterize the effects of diminished diastolic compliance. This computational model further suggests that biomechanical changes of the cardiac structure in the HFpEF may be a major driver of remodeling and may thus have considerable implications in the HFpEF hemodynamics and disease progression. Integration of a dynamic growth model with the fluid-structure interaction of the FEA simulation may be considered in future work to more comprehensively capture the dynamics of cardiac remodeling and hemodynamic aberrations induced by pressure overload. Moreover, further studies of the effects of active relaxation similar to Kadry et al.[30] and electrical conduction and contractility might be needed to simulate different phenotypes of diastolic dysfunction.

The development of simulation platforms that are suitable for studies of HFpEF is largely underreported in the literature. In this context, this work provides a unique environment for studies of the HFpEF pathophysiology. The anatomically derived lumped-parameter model will allow rapid simulation of the effect that varying patient-specific hemodynamic parameters (e.g., vascular luminal area and compliance) play in the global hemodynamics for healthy and HFpEF conditions. In addition, FEA modeling permits detailed investigation of the effects of temporal changes in mechanical properties and excitability of the heart tissue as they change progressively during HFpEF. Furthermore, the proposed models have potential utility for the simulation of novel therapies for HFpEF, partly addressing the lack of reliable in vivo, in vitro, and in silico models of HFpEF, which may be responsible for the suspension of clinical trials due to inadequate device optimization[42]. Finally, future work may involve the integration of these models into a single simulation by replacing the simplified lumped-parameter description underlying the FEA approach with the numerical solver model. This may further enhance the accuracy of these models and further support computational studies of HFpEF and other cardiovascular conditions.

In summary, two distinct computational models of HFpEF were described in this study. The ability of the developed platforms to describe baseline hemodynamics under physiologic conditions was first demonstrated. Then, the changes arising from aortic stenosis and ultimately from HFpEF due to left ventricular remodeling were investigated, demonstrating that the results were consistent

with those reported in the literature. Finally, the simulated hemodynamic conditions showed elevations in the cardiac wall stress in the HFpEF heart compared to physiologic conditions. In the context of the incredibly pressing healthcare challenge that HFpEF represents, these proposed platforms are among the first in silico descriptions that can provide insights into the hemodynamics and biomechanics of HFpEF. These computational models may be further used as a tool for the development of treatments for HFpEF, ultimately supporting translational research in the field.

ACKNOWLEDGMENTS:

We acknowledge funding from the Harvard-Massachusetts Institute of Technology Health Sciences and Technology program, and the SITA Foundation Award from the Institute for Medical Engineering and Science.

DISCLOSURES:

There are no conflicts of interest associated with this work.

REFERENCES:

1 Borlaug, B. A. & Paulus, W. J. Heart failure with preserved ejection fraction: Pathophysiology, diagnosis, and treatment. *European Heart Journal.* **32** (6), 670-679 (2011).

2 Borlaug, B. A., Kane, G. C., Melenovsky, V. & Olson, T. P. Abnormal right ventricular-pulmonary artery coupling with exercise in heart failure with preserved ejection fraction. *European Heart Journal.* **37** (43), 3293-3302 (2016).

3 Borlaug, B. A. Evaluation and management of heart failure with preserved ejection fraction. *Nature Reviews Cardiology.* **17** (9), 1-15 (2020).

4 Carabello, B. A. & Paulus, W. J. Aortic stenosis. *The Lancet.* **373** (9667), 956-966 (2009).

5 Lam, C. S. P., Donal, E., Kraigher-Krainer, E. & Vasan, R. S. Epidemiology and clinical course of heart failure with preserved ejection fraction. *European Journal of Heart Failure.* **13** (1), 18-28 (2011).

6 Omote, K. *et al.* Left ventricular outflow tract velocity time integral in hospitalized heart failure with preserved ejection fraction. *ESC Heart Failure.* **7** (1), 167-175 (2020).

7 Samson, R., Jaiswal, A., Ennezat, P. V., Cassidy, M. & Jemtel, T. H. L. Clinical phenotypes in heart failure with preserved ejection fraction. *Journal of the American Heart Association.* **5** (1), (2016).

8 Weber, K. T., Brilla, C. G. & Janicki, J. S. Myocardial fibrosis: Functional significance and regulatory factors. *Cardiovascular Research.* **27** (3), 341-348 (1993).

9 Borbély, A. *et al.* Cardiomyocyte stiffness in diastolic heart failure. *Circulation.* **111** (6), 774-781 (2005).

10 Borlaug, B. A., Lam, C. S. P., Roger, V. L., Rodeheffer, R. J. & Redfield, M. M. Contractility and Ventricular Systolic Stiffening in Hypertensive Heart Disease. Insights Into the Pathogenesis of Heart Failure With Preserved Ejection Fraction. *Journal of the American College of Cardiology.* **54** (5), 410-418 (2009).

11 Penicka, M. *et al.* Heart Failure With Preserved Ejection Fraction in Outpatients With Unexplained Dyspnea. A Pressure-Volume Loop Analysis. *Journal of the American College of Cardiology.* **55** (16), 1701-1710 (2010).

12 Owen, B., Bojdo, N., Jivkov, A., Keavney, B. & Revell, A. Structural modelling of the cardiovascular system. *Biomechanics and Modeling in Mechanobiology.* **17** (5), 1217-1242 (2018).
13 Zhou, S. *et al.* A review on low-dimensional physics-based models of systemic arteries: Application to estimation of central aortic pressure. *BioMedical Engineering Online.* **18** (1), 41 (2019).
14 Sagawa, K., Lie, R. K. & Schaefer, J. Translation of Otto frank's paper "Die Grundform des arteriellen Pulses" zeitschrift für biologie 37: 483-526 (1899). *Journal of Molecular and Cellular Cardiology.* **22** (3), 253-254 (1990).
15 Rosalia, L., Ozturk, C., Van Story, D., Horvath, M. & Roche, E. T. Object-oriented lumped-parameter modeling of the cardiovascular system for physiological and pathophysiological conditions. *Advanced theory and simulations,* In Press (2021).
16 Lopez-Perez, A., Sebastian, R. & Ferrero, J. M. Three-dimensional cardiac computational modelling: METHODS, features and applications. *BioMedical Engineering Online.* **14** 35 (2015).
17 Xie, X., Zheng, M., Wen, D., Li, Y. & Xie, S. A new CFD based non-invasive method for functional diagnosis of coronary stenosis. *BioMedical Engineering Online.* **17** (1), 36 (2018).
18 Abaqus Dassault, S. SIMULIA living heart human model user documentation. (2017).
19 Baillargeon, B., Rebelo, N., Fox, D. D., Taylor, R. L. & Kuhl, E. The living heart project: A robust and integrative simulator for human heart function. *European Journal of Mechanics, A/Solids.* **48** 38-47 (2014).
20 Moscato, F. *et al.* Use of continuous flow ventricular assist devices in patients with heart failure and a normal ejection fraction: a computer-simulation study. *The Journal of Thoracic and Cardiovascular Surgery.* **145** (5), 1352-1358 (2013).
21 Fresiello, L., Meyns, B., Di Molfetta, A. & Ferrari, G. A Model of the Cardiorespiratory Response to Aerobic Exercise in Healthy and Heart Failure Conditions. *Frontiers in Physiology.* **7** (189), (2016).
22 Moscato, F. *et al.* Left ventricle afterload impedance control by an axial flow ventricular assist device: a potential tool for ventricular recovery. *Artificial Organs.* **34** (9), 736-744 (2010).
23 Colacino, F. M., Moscato, F., Piedimonte, F., Arabia, M. & Danieli, G. A. Left ventricle load impedance control by apical VAD can help heart recovery and patient perfusion: a numerical study. *Asaio Journal.* **53** (3), 263-277 (2007).
24 Gu, K. *et al.* Lumped parameter model for heart failure with novel regulating mechanisms of peripheral resistance and vascular compliance. *Asaio Journal.* **58** (3), 223-231 (2012).
25 Suga, H., Sagawa, K. & Kostiuk, D. P. Controls of ventricular contractility assessed by pressure-volume ratio, Emax. *Cardiovascular Research.* **10** (5), 582-592 (1976).
26 Fernandez de Canete, J., Saz-Orozco, P. d., Moreno-Boza, D. & Duran-Venegas, E. Object-oriented modeling and simulation of the closed loop cardiovascular system by using SIMSCAPE. *Computers in Biology and Medicine.* **43** (4), 323-333 (2013).
27 Heldt, T., Shim, E. B., Kamm, R. D., Mark, R. G. & Massachusetts. Computational modeling of cardiovascular response to orthostatic stress. *Journal of Applied Physiology.* **92** (3), 1239-1254 (2002).
28 Granegger, M. *et al.* A Valveless Pulsatile Pump for the Treatment of Heart Failure with Preserved Ejection Fraction: A Simulation Study. *Cardiovascular Engineering and Technology.* **10** (1), 69-79 (2019).
29 Hay, I., Rich, J., Ferber, P., Burkhoff, D. & Maurer, M. S. Role of impaired myocardial

relaxation in the production of elevated left ventricular filling pressure. *American Journal of Physiology-Heart and Circulatory Physiology.* **288** (3), H1203-1208 (2005).
30 Kadry, K. *et al.* Biomechanics of diastolic dysfunction: a one-dimensional computational modeling approach. *American Journal of Physiology-Heart and Circulatory Physiology.* **319** (4), H882-H892 (2020).
31 Luo, C., Ramachandran, D., Ware, D. L., Ma, T. S. & Clark, J. W., Jr. Modeling left ventricular diastolic dysfunction: classification and key indicators. *Theoretical Biology & Medical Modelling.* **8** 14-14 (2011).
32 Burkhoff, D. *et al.* Left atrial decompression pump for severe heart failure with preserved ejection fraction: theoretical and clinical considerations. *JACC: Heart Failure.* **3** (4), 275-282 (2015).
33 Ahmad Bakir, A., Al Abed, A., Stevens, M. C., Lovell, N. H. & Dokos, S. A Multiphysics Biventricular Cardiac Model: Simulations With a Left-Ventricular Assist Device. *Frontiers in Physiology.* **9** (1259), (2018).
34 Genet, M., Lee, L. C., Baillargeon, B., Guccione, J. M. & Kuhl, E. Modeling pathologies of diastolic and systolic heart failure. *Annals of Biomedical Engineering.* **44** (1), 112-127 (2016).
35 Sack, K. L. *et al.* Investigating the Role of Interventricular Interdependence in Development of Right Heart Dysfunction During LVAD Support: A Patient-Specific Methods-Based Approach. *Frontiers in Physiology.* **9** (520), (2018).
36 Baillargeon, B. *et al.* Human cardiac function simulator for the optimal design of a novel annuloplasty ring with a sub-valvular element for correction of ischemic mitral regurgitation. *Cardiovascular Engineering and Technology.* **6** (2), 105-116 (2015).
37 Sack, K. L. *et al.* Partial LVAD Restores Ventricular Outputs and Normalizes LV but not RV Stress Distributions in the Acutely Failing Heart in Silico. *The International Journal of Artificial Organs.* **39** (8), 421-430 (2016).
38 Baumgartner, H. *et al.* Echocardiographic assessment of valve stenosis: EAE/ASE recommendations for clinical practice. *Journal of the American Society of Echocardiography.* **22** (1), 1-23 (2009).
39 Rajani, R., Hancock, J. & Chambers, J. The art of assessing aortic stenosis. *Heart.* **98** iv14-iv22 (2012).
40 Vahanian, A. *et al.* Guidelines on the management of valvular heart disease: The Task Force on the Management of Valvular Heart Disease of the European Society of Cardiology. *European Heart Journal.* **28** (2), 230-268 (2007).
41 Matiwala, S. & Margulies, K. B. Mechanical approaches to alter remodeling. *Current Heart Failure Reports.* **1** (1), 14-18 (2004).
42 NIH Clinical Trials Registry, ImCardia for DHF to Treat Diastolic Heart Failure (DHF) Patient a Pilot Study (ImCardia). (2011).

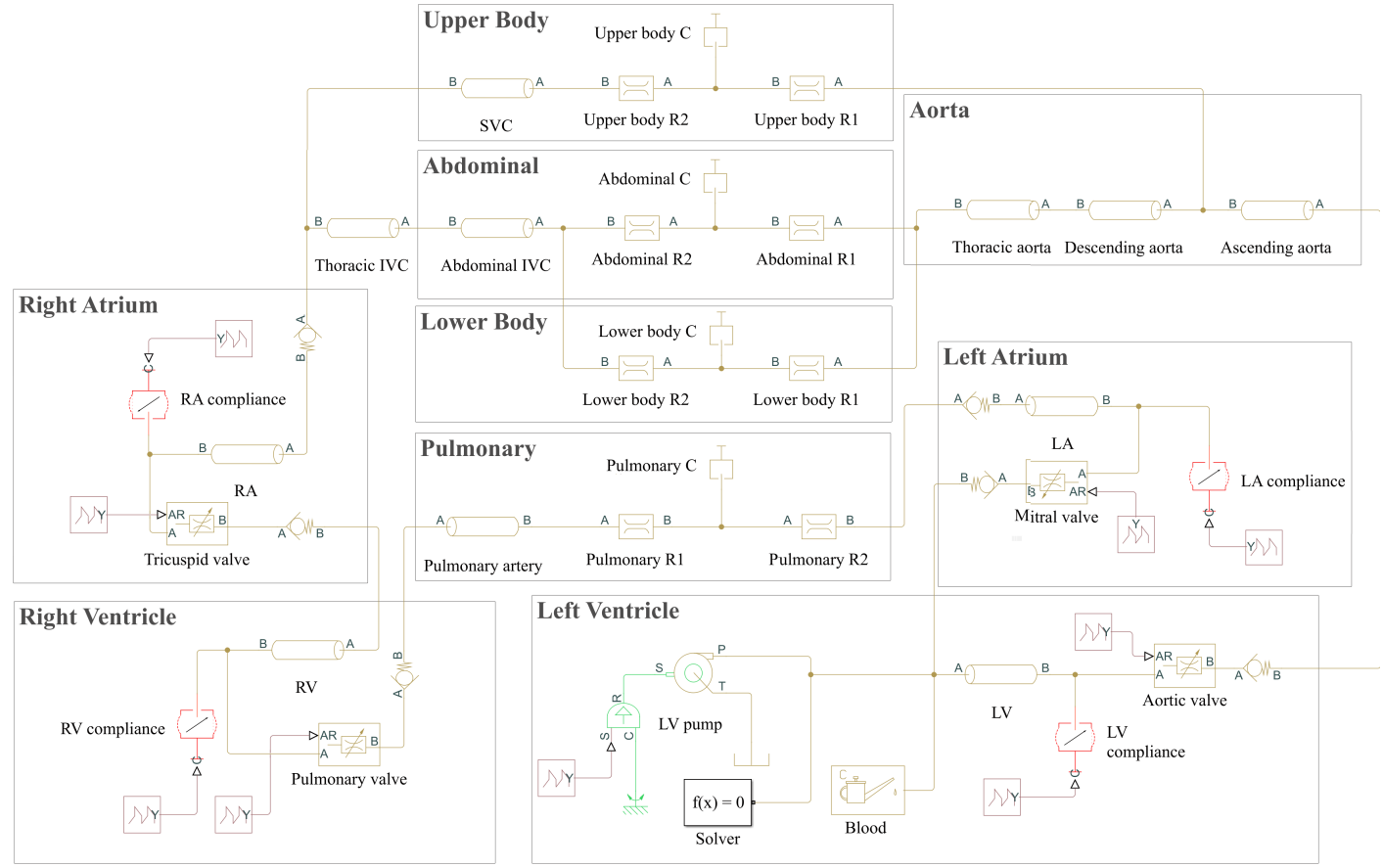

Figure 2

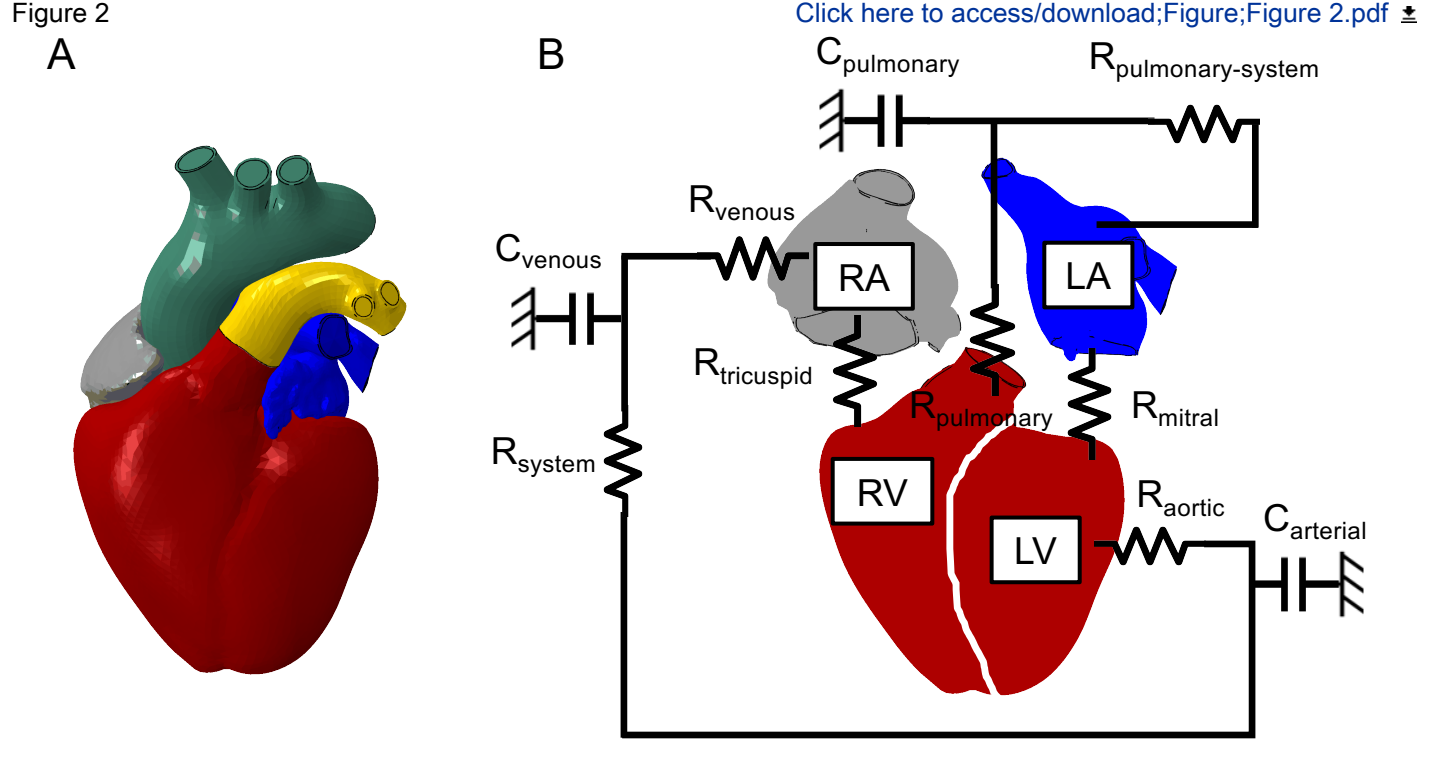

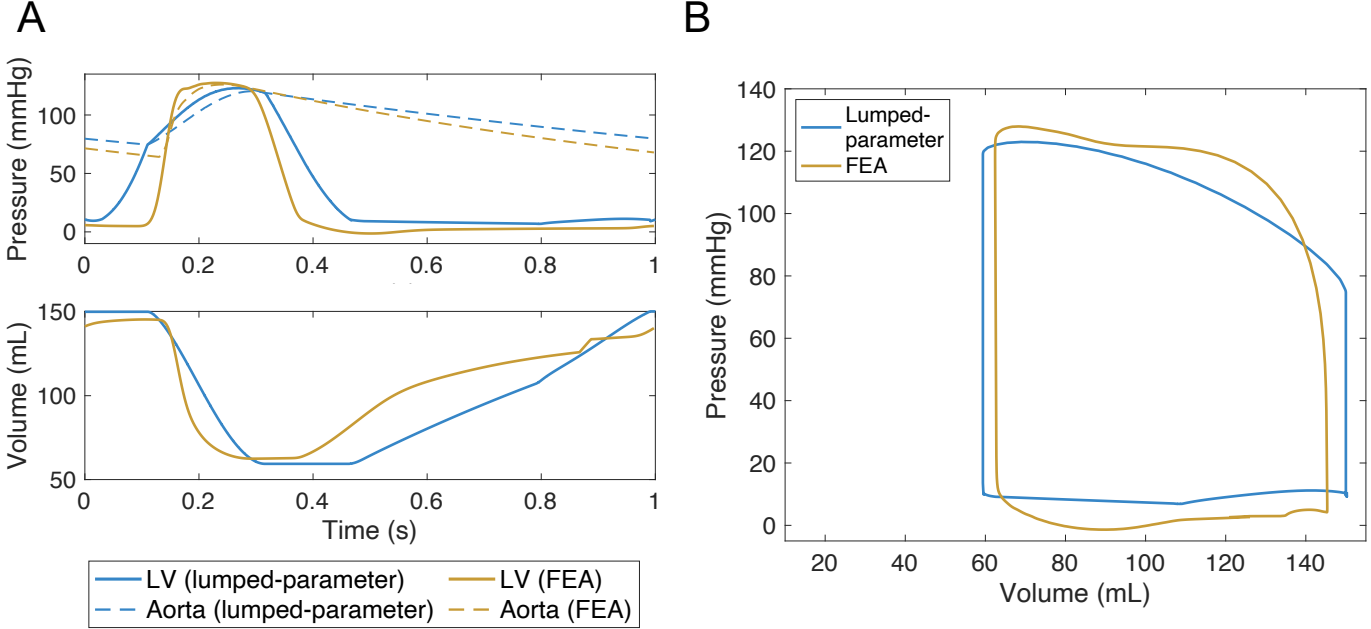
A
Pressure (mmHg)
100
50
0
0
0.2
0.4
0.6
0.8
1
Volume (mL)
150
100
50
0
0.2
0.4
0.6
0.8
1
Time (s)
LV (lumped-parameter)
LV (FEA)
Aorta (lumped-parameter)
Aorta (FEA)
B
Pressure (mmHg)
140
120
100
80
60
40
20
0
20
40
60
80
100
120
140
Volume (mL)
Lumped-parameter
FEA

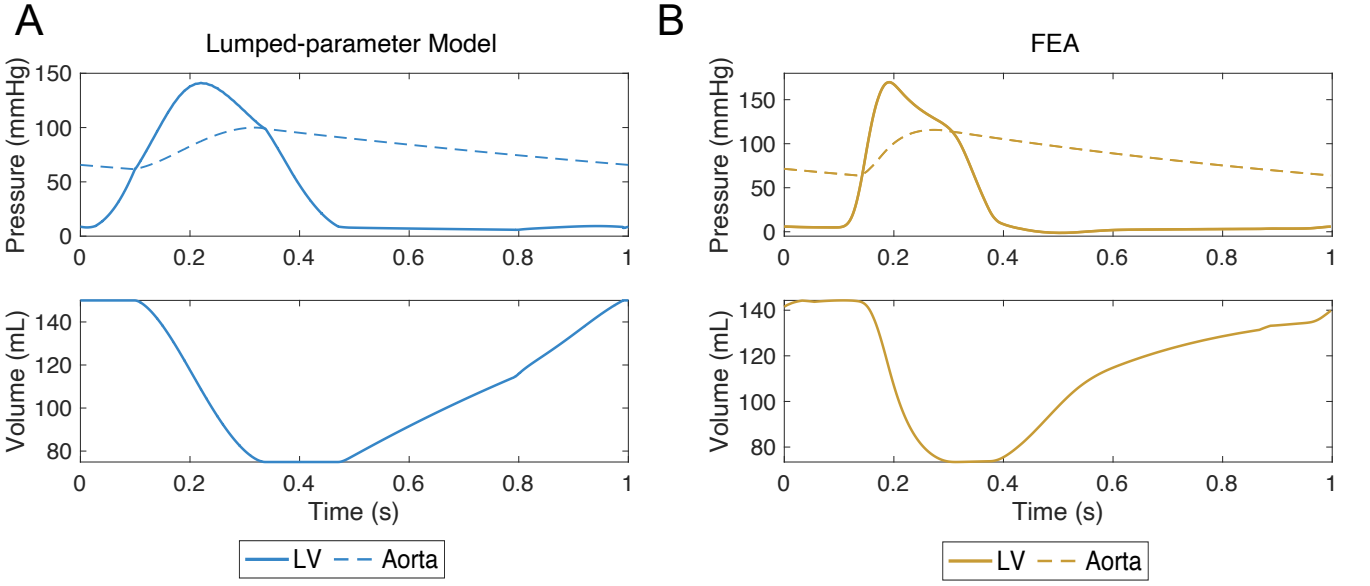
A
Lumped-parameter Model
Pressure (mmHg)
150
100
50
0
0
0.2
0.4
0.6
0.8
1
Volume (mL)
140
120
100
80
Time (s)
LV
Aorta
B
FEA
Pressure (mmHg)
Volume (mL)
Time (s)
LV
Aorta

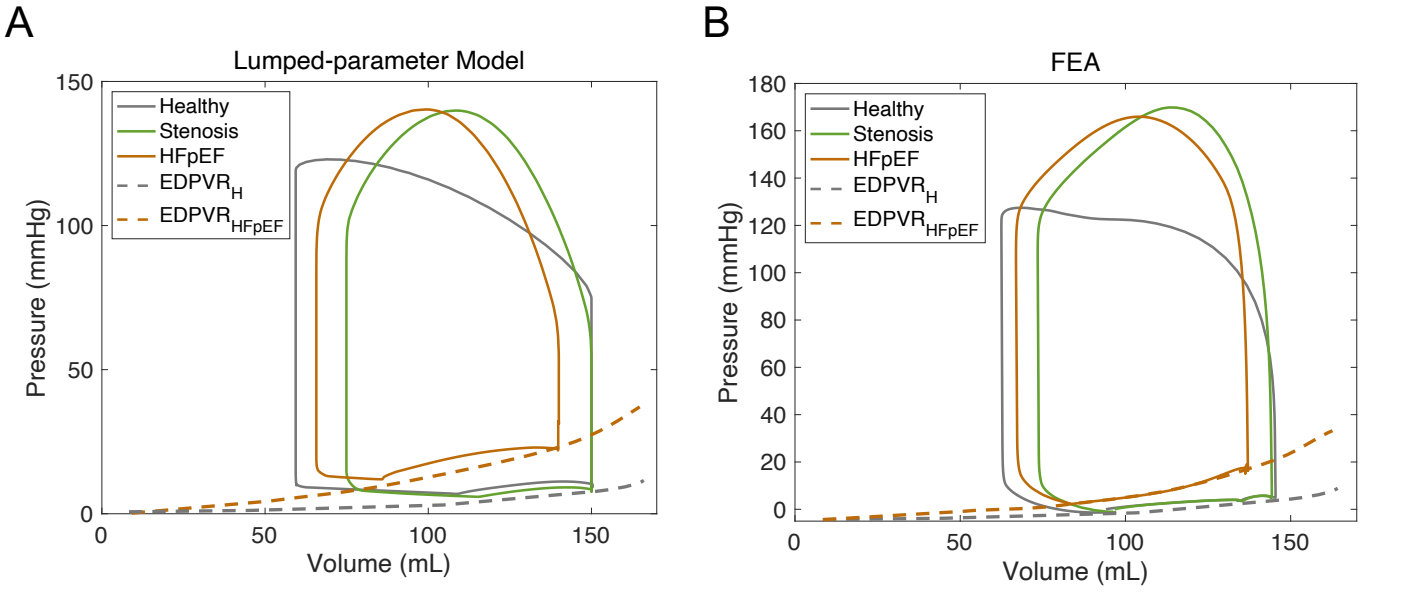
A
Lumped-parameter Model
Healthy
Stenosis
HFpEF
EDPVR$_H$
EDPVR$_{HFpEF}$
Pressure (mmHg)
Volume (mL)
0
50
100
150
B
FEA
Healthy
Stenosis
HFpEF
EDPVR$_H$
EDPVR$_{HFpEF}$
Pressure (mmHg)
Volume (mL)
0
20
40
60
80
100
120
140
160
180

Healthy

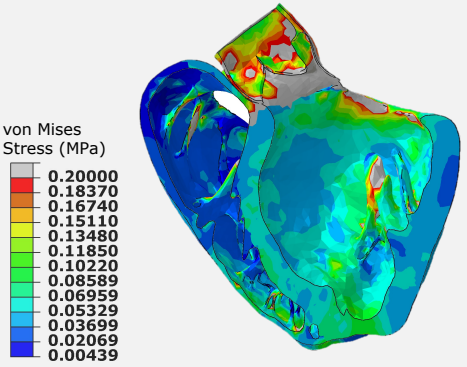

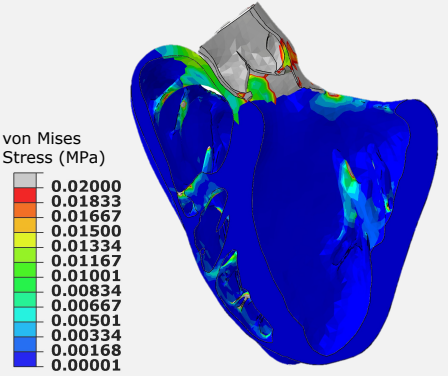

HFpEF

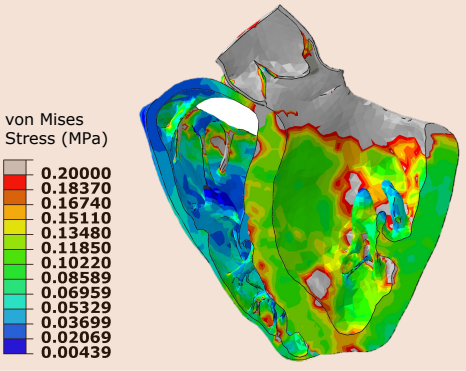

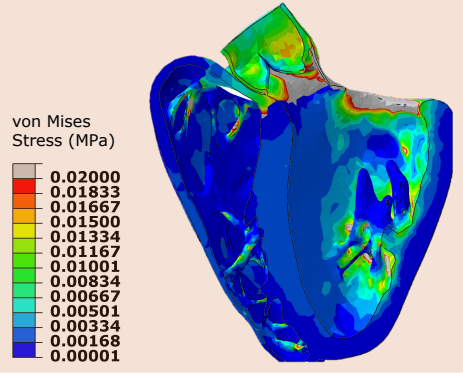

Systole

Diastole

Table of Materials

Click here to access/download;Table of Materials;Rosalia_JoVE_Table_of_Materials_R1 (1).xlsx

Name of Material/Equipment	Company	Catalog Number	Comments/Description
Abaqus Software	Dassault Systèmes Simulia Corp.		Version used: 2018; FEA simulation software
HETVAL	Dassault Systèmes Simulia Corp.		Version used: 2018
Hydraulic (Isothermal) library	MathWorks		Version used: 2020a
Living Heart Human Model	Dassault Systèmes Simulia Corp.		Version used: V2_1, anatomically accurate FEA platform of 4-chamber adult human heart
MATLAB	MathWorks		Version used: 2020a, object-oriented numerical solver
SIMSCAPE FLUIDS	MathWorks		
UAMP	Dassault Systèmes Simulia Corp.		Version used: 2018
VUANISOHYPER	Dassault Systèmes Simulia Corp.		Version used: 2018

Massachusetts Institute of Technology
Department of Mechanical Engineering
Street Address, Building E25-344
Cambridge, MA 02139

Ellen Roche, PhD
Asst. Professor
W.M. Keck Foundation Career Development Professor
e: etr@mit.edu
t: 617-258-6024

Date: January 19th, 2021

Re: Manuscript (JoVE62167) entitled "Lumped-parameter and finite element modeling of heart failure with preserved-ejection fraction." Luca Rosalia, Caglar Ozturk, Ellen T. Roche

Dear Dr. Vidhya Iyer,

We would like to thank you for your comments relative to our manuscript entitled **"Lumped-parameter and finite element modeling of heart failure with preserved-ejection fraction"** (Manuscript #: JoVE62167), submitted for consideration as an original research article as part of the method collection entitled *Approaches for preclinical studies of heart failure with preserved ejection fraction (HFpEF)* in *JoVE*. Your comments have been addressed in the revised version of the manuscript.

We would also like to thank you again for letting us include the reference to our work, currently in editorial revision, to the manuscript submitted to your journal. The final round of revision of that work has been already submitted, and we are confident that it will soon be accepted for publication. The lumped-parameter model described in this *JoVE* manuscript is based on a new platform and uses object-oriented elements that were first described in the referenced research article. The *JoVE* manuscript utilizes this platform to simulate a specific pathophysiological condition, namely Heart Failure with Preserved Ejection Fraction. For these reasons, we believe it is important that our other work (Ref#15) can still be referenced in the manuscript and we are very grateful that you are allowing us to do so. If it is published before the *JoVE* manuscript, we will be sure to update you.

We would like to thank you again for considering our work and for the helpful comments and suggestions to enhance the quality of the work.

Please do not hesitate to contact me if there are any questions. Thank you for your consideration.

Sincerely,

etr@mit.edu, Phone +1 617 258 6024

Ellen Roche Asst. Professor

Dept. of Mechanical Engineering Massachusetts Institute of Technology and Institute for Medical Engineering and Science etr@mit.edu

SUPPLEMENTAL FILE

TITLE:
Lumped-Parameter and Finite Element Modeling of Heart Failure with Preserved Ejection Fraction

AUTHORS AND AFFILIATIONS:
Luca Rosalia[1,2], Caglar Ozturk[1], Ellen T. Roche[1,2,3]

[1]Institute for Medical Engineering and Science, Massachusetts Institute of Technology, Cambridge, Massachusetts 02139, USA
[2]Health Science and Technology Program, Harvard/Massachusetts Institute of Technology, Cambridge, Massachusetts 02139, USA
[3]Department of Mechanical Engineering, Massachusetts Institute of Technology, Cambridge, Massachusetts 02139, USA

L.R. and C.O. contributed equally to this work.

Luca Rosalia (lros@mit.edu)
Caglar Ozturk (cozturk@mit.edu)

Corresponding author:
Ellen T. Roche (etr@mit.edu)

Lumped-parameter hydraulics (isothermal) library: Details on the elements used in the lumped-parameter simulation can be found here.

Table S1: Geometric and mechanical parameters of baseline lumped-parameter simulation.

	Density [kg m^{-3}][1]	Kinematic viscosity [mm^2 s^{-1}][1]	Bulk modulus [GPa][2]
Blood	1060	3.55	2.2
	Diameter [cm][3-6]	Length [cm][3-5,7-9]	Compliance [m Pa^{-1}]
Left ventricle	4.4	7	$0.002–1 \times 10^{-6}$
Right ventricle	4.8	5	$1.8–5.5 \times 10^{-5}$
Left atrium	5	7.5	$0.8–1.7 \times 10^{-5}$
Right atrium	5.6	5	$1.9–2.3 \times 10^{-5}$
Ascending aorta	2.65	8.8	4.0×10^{-7}
Descending aorta	2.15	6.9	7.0×10^{-7}
Thoracic aorta	1.92	33.2	1.7×10^{-7}
Pulmonary artery	3	5	2.2×10^{-7}
Superior vena cava (SVC)	2.1	7.1	5.0×10^{-6}
Abdominal inferior vena cava (IVC)	1.4	17	4.4×10^{-6}
Thoracic IVC	1.4	2.5	6.4×10^{-7}
	Area [cm^2][10-13]	Opening time [s]	Closing time [s]
Aortic valve	4	0.00	0.43
Pulmonary valve	5	0.00	0.47
Mitral valve	4.2	0.53	1.00
Tricuspid valve	5	0.43	1.00
	Resistance [Pa s m^{-3}][14,15]	Volume [L][14]	Compliance [m Pa^{-1}]
Upper body	$0.31–5.2 \times 10^8$	0.89	6.7×10^{-8}
Abdominal	$0.15–2.3 \times 10^8$	2.02	3.6×10^{-8}
Lower body	$0.40–4.7 \times 10^8$	0.51	4.1×10^{-8}
Pulmonary	$0.50–5.0\ 10^6$	0.55	6×10^{-7}

Table S2: Extensive set of parameters of baseline lumped-parameter simulation.

	Relative amount of trapped air					
Custom hydraulic fluid	0.005					
	Laminar friction constant	Aggregate equivalent length [m]	Internal surface roughness height [μm]	Laminar flow upper Reynolds limit	Turbulent flow upper Reynolds limit	Specific heat ratio
Hydraulic pipeline	64	0	15	2000	4000	1.4
	Viscoelastic time constant [s]			Specific heat ratio		
Constant volume hydraulic chamber	0.01			1.4		
Variable-compliance compliance chamber	0.01			1.4		
	First approximating coefficient [Pa kg^{-1} m^3]	Second approximating coefficient [Pa s kg^{-1}]	Third approximating coefficient [Pa s^2 kg^{-1} m^{-3}]	Fourth approximating coefficient [Pa s^2 kg^{-1} m^{-3}]	Correction factor	Pump design delivery [L min^{-1}]
Centrifugal pump	326.8	3.104×10^4	1.097×10^7	2.136×10^5	0.8	130
	Reference angular velocity [rpm]	Reference density [kg m^{-3}]	Leak resistance [Pa m^3 s^{-1}]	Drive shaft torque [N m]	Torque-pressure coefficient [N m Pa^{-1}]	Angular speed threshold for flow reversal [rad s^{-1}]
Centrifugal pump	1770	1060	7×10^6	0.1	1×10^{-6}	1×10^{-9}

	Maximum passage area [m^2]	Crack pressure [Pa]	Maximum opening pressure [Pa]	Flow discharge coefficient	Leakage [m^2]	Laminar flow pressure ratio
Check valve	0.1	0.01	0.1	1	1×10^{-12}	0.999

	Flow discharge coefficient	Minimum area	Laminar flow pressure ratio
Variable area hydraulic orifice	1	1×10^{-15}	0.999

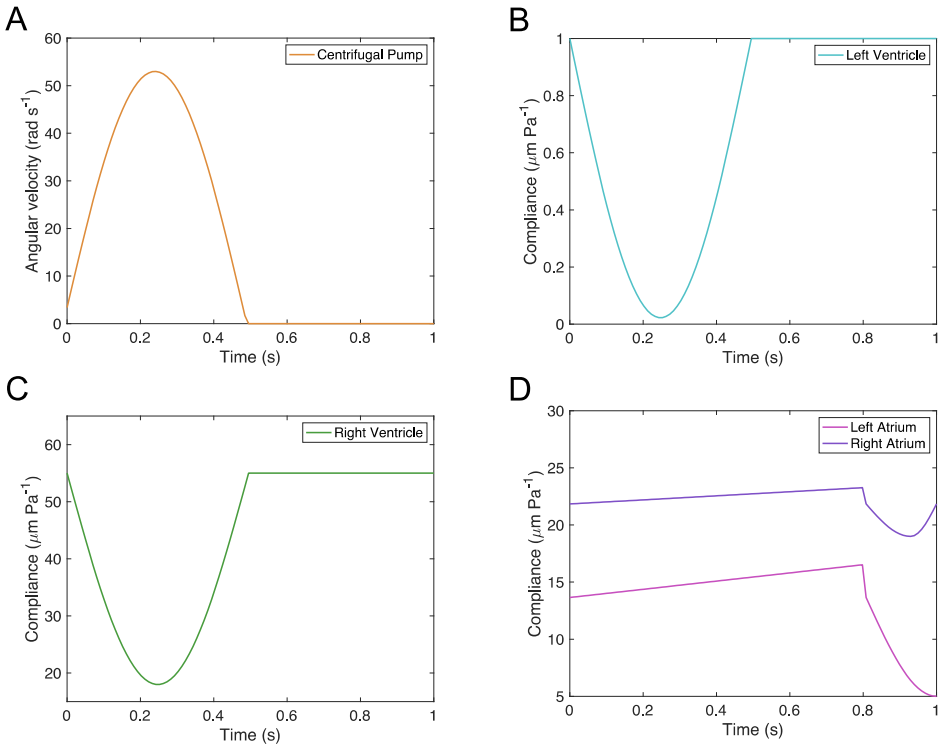

Figure S1: Input signals for (**A**) centrifugal pump, (**B**) left ventricle, (**C**) right ventricle, (**D**) left and right atria for the lumped-parameter simulation.

Table S3: Fluid cavities values in the mechanical finite element analysis (FEA) model[3].

Boundary Name	Pressure (MPa)
CAV-ARTERIAL-COMP	1.06×10^{-2}
CAV-VENOUS-COMP	2.66×10^{-4}
CAV-PULMONARY-COMP	1.06×10^{-3}
CAV-LV	5.33×10^{-4}
CAV-RV	2.66×10^{-4}
CAV-AORTA	1.06×10^{-2}
CAV-PULMONARY_TRUNK	1.06×10^{-3}
CAV-RA	2.66×10^{-4}
CAV-LA	5.33×10^{-4}
CAV-SVC	2.66×10^{-4}

Table S4: Boundary conditions of fluid exchange links for the finite element analysis (FEA) model.

Boundary Name	Viscous Resistance Coefficient Value ($1/mm^2$)
Link-Aortic-Valve	112896
Link-Body-Resistance	59965.5
Link-Mitral-Valve	2359.04
Link-Pulmonary-Resistance	4750
Link-Pulmonary-Valve	423.47
Link-Tricuspid-Valve	429.5
Link-Venous-Resistance	429.5

FEA simulations were performed by the FEA simulation software. **Table S5** shows the required model files to run the simulation. More details can be found in the User Guide[3].

Table S5: The required simulation files for the finite element analysis (FEA) model[3].

File Name	Description
LH-Human-Model-Beta-V2_1.cae	FEA simulation software GUI File
nodes_AORTIC_ARCH.inp	Initial nodal coordinates of aortic arch
nodes_VENTRICLES.inp	Initial nodal coordinates of right and left ventricles
nodes_TRICUSPIDVALVE_MESH.inp	Initial nodal coordinates of tricuspid valve
nodes_PULMONARY_VALVE_CUT.inp	Initial nodal coordinates of pulmonary valve
nodes_R_ATRIUM.inp	Initial nodal coordinates of the right atrium
nodes_PULMONARY_TRUNK.inp	Initial nodal coordinates of the pulmonary cavity
nodes_MITRALVALVE_MESH.inp	Initial nodal coordinates of the mitral valve
nodes_L_ATRIUM.inp	Initial nodal coordinates of the left atrium
nodes_ASSEMBLY.inp	Initial nodal coordinates of the assembly connections
nodes_AORTIC_VALVE_CUT.inp	Initial nodal coordinates of the aortic valve
nodes_CHORDAE_TENDINEAE_MITRAL.inp	Initial nodal coordinates of the MV chordae tendineae
nodes_CHORDAE_TENDINEAE_TRICUSPID.inp	Initial nodal coordinates of the TV chordae tendineae
DF-Aortic_Arch.inp	Discrete field file of the aortic arch for the fiber orientations
DF-L_Atrium.inp	Discrete field file of the left atrium for the fiber orientations
DF-MITRALVALVE_MESH.inp	Discrete field file of the mitral valve for the fiber orientations
DF-Pulmonary_Trunk.inp	Discrete field file of the pulmonary cavity for the fiber orientations
DF-R_Atrium.inp	Discrete field file of the right atrium for the fiber orientations
DF-TRICUSPIDVALVE_MESH.inp	Discrete field file of the tricuspid valve for the fiber orientations
DF-Ventricles.inp	Discrete field file of the ventricles for the fiber orientations
mech-mat-ARTERY.inp	Material definition input for the artery in mechanical simulation
mech-mat-LA_ACTIVE.inp	Material definition input for the active left atrium components in mechanical simulation

mech-mat-LV_ACTIVE.inp	Material definition input for the active left ventricle components in mechanical simulation
mech-mat-PASSIVE.inp	Material definition input for the passive cardiac tissue components in mechanical simulation
mech-mat-RA_ACTIVE.inp	Material definition input for the active right atrium components in mechanical simulation
mech-mat-RV_ACTIVE.inp	Material definition input for the active right ventricle components in mechanical simulation
mech-mat-VALVE.inp	Material definition input for the valves in mechanical simulation
elec-mat-L_Atrium.inp	Material definition input for the left atrium in electrical simulation
elec-mat-PurkinjeL.inp	Material definition input for the Prukinje fiber in electrical simulation
elec-mat-PurkinjeR.inp	Material definition input for the Prukinje fiber in electrical simulation
elec-mat-R_Atrium.inp	Material definition input for the right atrium in electrical simulation
elec-mat-Resistors.inp	Material definition input for the conduction elements in electrical simulation
elec-mat-Ventricles.inp	Material definition input for the ventricles in electrical simulation
standardU.dll	FEA sImulation software library and subroutine files
heart-elec-std.obj	
explicitU-D.dll	
heart-mech-xplD.obj	
libstandardU.so	
heart-elec-std.o	
libexplicitU-D.so	
heart-mech-xplD.o	
abaqus_v6.env	
calcNodeCoords.py	FEA simulation software toolbox files
inversePreliminary.py	
straight_mv_chordae.py	
genPartFile.py	
genAssemblyFile.py	

The fluid flow between heart chambers is modeled using fluid exchange definitions. The fluid exchange module (FEA Simulation software) was employed to create the lumped-parameter model of blood flow depicted in **Figure 2B**. This model utilizes the conventional RC circuit analogy, which, in its simplest form, can be written as:

$$\mathrm{i} = \frac{V}{R} \tag{S1}$$

where i is current, V is voltage and R is resistance. In the hydraulic domain, **Equation S1** can be rewritten as:

$$\mathrm{Q} = \frac{\Delta P}{R} \tag{S2}$$

where Q represents the volume of blood per unit time, ΔP is pressure gradient across a conduit and R is resistance to flow. In the FEA model, fluid exchange is defined as fluid flow through porous media as per Darcy's Law (**Equation S3**). Flow is assumed to be laminar, and it is characterized by viscous loss coefficients in the linear flow direction[16]:

$$Q = \frac{-kA}{\mu}\frac{\Delta P}{L} \tag{S3}$$

where Q is the volumetric flow rate, k is the permeability of porous media, μ is the dynamic viscosity, A is the cross-sectional area, and L is the length over which pressure drop occurs. This can be simplified and rewritten as in **Equation S4**:

$$\Delta P = \frac{\rho}{\alpha A} Q \tag{S4}$$

where 1/α is equal to the viscous resistance coefficient C_v[16], yielding:

$$\Delta P = \frac{\rho C_v}{A} Q \tag{S5}$$

In the FEA model, the viscous resistance coefficient C_v is implemented as an input parameter to calculate the flow and pressure drop between fluid cavities.

Table S6: Parameters for the aortic-stenosis lumped-parameter simulation.

	Area [cm^2]	Opening time [s]	Closing time [s]
Aortic valve	1.2	0.00	0.43

Table S7: Fluid exchange link definitions in the finite element analysis (FEA) model[3].

Fluid Exchange Name	Effective Exchange Area (mm^2)	
	Normal Heart	Aortic Stenosis
LINK-ARTERIAL-VENOUS	441.15	441.15
LINK-LA-LV	1039.8	1039.8
LINK-LV-ARTERIAL	440	132
LINK-PULMONARY-LA	434.9	434.9
LINK-RA-RV	1722.2	1722.2
LINK-RV-PULMONARY	434.9	434.9
LINK-VENOUS-RA	441.15	441.15

Table S8: Parameters for the HFpEF lumped-parameter simulation.

	Diameter [cm]	Length [cm]	End-Diastolic Compliance [m Pa^{-1}]
Left ventricle	4.4	7	2.2×10^{-12}
	Area [cm^2]	Opening time [s]	Closing time [s]
Aortic valve	1.2	0.00	0.43
	Leak resistance [Pa m^3 s^{-1}]		
Centrifugal pump	18×10^6		

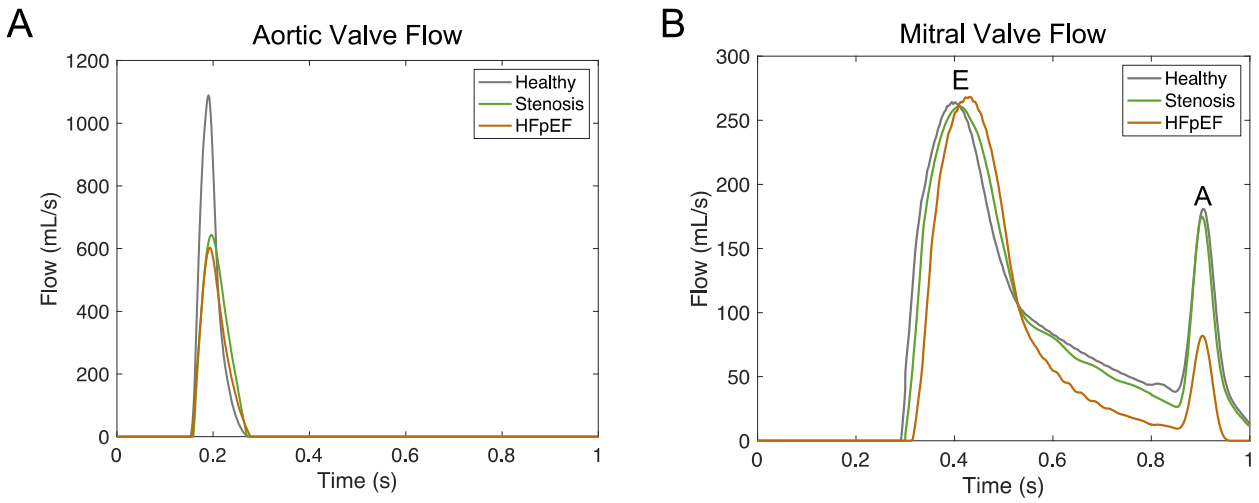

Figure S2: (**A**) Aortic and (**B**) mitral flow signals for the baseline, stenosis, and HFpEF profiles, obtained by FEA. Abbreviations: E = early relaxation phase; A = atrial contraction; FEA = finite element analysis; HFpEF = heart failure with preserved ejection fraction.

REFERENCES

1 van Wyk, S., Prahl Wittberg, L., Bulusu, K. V., Fuchs, L., Plesniak, M. W. Non-Newtonian perspectives on pulsatile blood-analog flows in a 180° curved artery model. *Physics of Fluids.* **27** (7), 71901–71901 (2015).

2 Carew, T. E., Vaishnav, R. N., Patel, D. J. Compressibility of the arterial wall. *Circulation research.* **23** (1), 61–68 (1968).

3 Abaqus Dassault, S. SIMULIA living heart human model user documentation. (2017).

4 Cuomo, F. et al. Effects of age-associated regional changes in aortic stiffness on human hemodynamics revealed by computational modeling. *PLoS ONE.* 12 (3), e0173177 (2017).

5 Sonavane, S. K. et al. Comprehensive imaging review of the superior vena cava. *RadioGraphics*. **35**, 1875–1892 (2015).
6 Patil, S. et al. Assessment of inferior vena cava diameter by echocardiography in normal Indian population: A prospective observational study. *Indian Heart Journal.* **68** (Suppl 3), S26–S30 (2016).
7 Dotter, C. T., Roberts, D. J., Steinberg, I. Aortic length: angiocardiographic measurements. *Circulation.* **2** (6), 915–920 (1950).
8 Ghosh, S. K., Paul, S. Anatomy of the retrohepatic segment of the inferior vena cava and the ostia venae hepaticae with its clinical significance. *Surgical and Radiologic Anatomy.* **34**, 347–355 (2012).
9 Mozes, G., Gloviczki, P. *The vein book*. Bergan, J. J.(ed), Academic Press, 15–25 (2007).
10 González-Mansilla, A. et al. Valve area and the risk of overestimating aortic stenosis. *Heart.* **105** (12), 911–919 (2019).
11 Capps, S. B., Elkins, R. C., Fronk, D. M. Body surface area as a predictor of aortic and pulmonary valve diameter. *The Journal of thoracic and cardiovascular surgery.* **119** (5), 975–982 (2000).
12 Soeki, T. et al. Mitral inflow and mitral annular motion velocities in patients with mitral annular calcification: evaluation by pulsed Doppler echocardiography and pulsed Doppler tissue imaging. *European Journal of Echocardiography.* **3** (2), 128–134 (2002).
13 Bhatia, A. Transesophageal echocardiography evaluation of tricuspid and pulmonic valves. *Annals of Cardiac Anaesthesia.* **19** (Supplement), S21–S25 (2016).
14 Heldt, T., Shim, E. B., Kamm, R. D., Mark, R. G. Computational modeling of cardiovascular response to orthostatic stress. *Journal of Applied Physiology.* 92 (3), 1239–1254 (2002).
15 Lilly, L. S. *Pathophysiology of heart disease: a collaborative project of medical students and faculty*. Lippincott Williams & Wilkins (2012).
16 Zeng, Z., Grigg, R. A criterion for non-Darcy flow in porous media. *Transport in porous media.* **63** (1), 57–69 (2006).